OpenFOAM® Journal

Volume 2 [Full Papers], Pages 13–30
ISSN: 2753-8168

COMPARISON OF OVERSET MESH WITH MORPHING MESH: FLOW OVER A FORCED OSCILLATING AND FREELY OSCILLATING 2D CYLINDER

MICHAEL ALLETTO

Private person
Email address: michael.alletto@gmx.de

DOI: 10.51560/ofj.v2.47
Version(s): OpenFOAM® v2006
Repo: -

Abstract. Fluid structural interactions involve temporal change of the boundaries of the computational domain as a result of the fluid forces acting on the solid structure. In order to take into account this change, OpenFOAM offers two different methods: the overset method and the morphing mesh method. The morphing mesh method takes into account the boundary movement by changing the topology of the mesh but keeping the connectivity between cells unchanged. The overset methods consists in non overlapping meshes which are moving relative to a background mesh. Usually the meshes do not change the topology. The coupling between meshes is achieved by interpolation of the variables between the meshes. Both methods are compared with each other and reference experiments and simulation by taking a two-dimensional laminar flow around a cylinder. The results are found to agree reasonable well with the references. Both mesh types give similar results for similar number of cells.

1. Introduction

Fluid structure interaction is associated with a multitude of physical phenomena: the stability and response of aircraft wings, the flow through arteries, the vibration of heat exchanger, the vibration of compressor and turbine blades and many more [1]. OpenFOAM offers two type of solvers two deal with the deformation of the structure (actually the deformation of a bounding surface): morphing mesh solvers and overset solvers. The class of morphing mesh solvers update the position of the vertices forming the cell in order to follow the motion of a boundary surface, i.e., the topology of the mesh is changed. The connectivity between the cells is kept unchanged. See [2] for an overview. Regarding the overset method, there is a static (not moving) background mesh and one or more meshes attached to the moving bodies. Usually, both meshes do not change their topology. In order to couple the solutions of both meshes, the variables are interpolated between the cells closed to the boundary of the moving mesh and the static background mesh. For a description of the method see e.g. [3, 4].

Fluid structure problems are characterized by a mutual influence of the fluid phase and the deforming solid: The fluid exerts a force on the solid via the pressure and surface stress distribution on the solid boundary. This forces lead to a deformation or position change of the surface. The change of the surface shape or position influences the flow motion. In order to capture the phenomena associated with moving boundaries accurately, it is important to carefully validate both fluid and structure solvers first separately and after that both together. In this spirit, we will first analyze the solvers used in OpenFOAM to solve fluid-structure interaction separately and then together. The chosen configuration consists in a circular cylinder in a two dimensional laminar flow. Despite its simplicity and the reduced computational costs (we need only a 2D mesh) this configuration is associated with a variety of interesting phenomena. For this reason it is an ideal test case to have a first impression about the accuracy and performance of the two method implemented in OpenFOAM to deal with displacing boundaries.

The first step in this validation is to look at the structure part of OpenFOAM solely. OpenFOAM uses a six degree of freedom solver to advance the location and orientation of a rigid body subject to fluid forces and restrains like springs and damper in time. The solver solves a set of ordinary differential which are derived from Newtons second law. For a case without fluid forces analytical solution exist which can be compared with the numerical results.

Received: 16 July 2021, Accepted: 12 January 2022, Published: 24 January 2022

As second step we will examine the inline oscillatory motion of a cylinder in a uniform flow. Inline means that the cylinder is oscillating parallel to the incoming flow by a prescribed motion. This kind of configuration is often used to validate solvers aiming to simulate large body motions (see e.g. [5, 6, 7]). In the works of Su et al. [5] and Liau et al. [6] the inline oscillation cylinder was one of the test cases to validate their immersed boundary method code. Chandar et al. [7] used this configuration (among others) to validate the OpenFOAM based overset method. The reason is that that despite its simplicity this configuration is associated with a variety of complex physical phenomena. One of this phenomena is frequency lock in: When the frequency of the oscillating cylinder is close to twice the shedding frequency of the stationary cylinder f_{st}, the frequency of the vortices shed became equal to the one of the cylinder. The amplitude of the cylinder motion which is required to maintain the lock in regime is increasing with departure from twice the shedding frequency of a fixed cylinder [8]. Another interesting phenomena is the increase of the lift coefficient C_l when the cylinder is oscillating at $2f_{st}$ [9]. For frequencies which are either lower or higher than $2f_{st}$, C_l is much lower [9]. Leontini et al. [10] made simulations with an in line oscillating cylinder at a Reynolds number of Re = 175. For this Re number the flow around a fixed cylinder is two dimensional. For an oscillation frequency f_c of $2f_{st}$ and an amplitude of 65% of the cylinder diameter the number of peaks in the frequency spectrum of the lift force increases considerably. For lower amplitudes of the oscillation only a few peaks are present in the frequency spectrum. Regarding OpenFOAM simulation of this particular configuration, only one work is known to the author of the present article. It is the work of Chandar et al. [7]. They used OpenFOAM together with an in-house developed overset library OPERA. They focused the attention on the numerical oscillations of the lift and drag generated by the overset interpolation rather than performing a comparison with reference experiments or simulations. Unfortunately no work was found using this test case with the morphing mesh method implemented in OpenFOAM.

In the third part of our validation study will examine the capability of OpenFOAM to simulate the vortex induced vibration on a circular cylinder in a 2D laminar configuration. The cylinder is free to vibrate in stream wise and in transverse direction. This kind of flow configuration is often used to validate codes which aim to describe the interaction of a fluid with a solid structure (see e.g. [11, 12]). Besides that, this configuration is used to answer fundamental questions of the basic physical mechanisms playing a role in the interaction between the flow and the solid body (see e.g. [13]). Recent studies concentrate on the phenomena which lead to large amplitude oscillation of the cylinder and the synchronization of the vortex shedding frequency with the natural frequency of the spring-mass-damper system (see [14, 15]). Regarding OpenFOAM specific simulation of this test case, the author could only find the PhD thesis of Conceição [16]. He performed a systematic validation of the one and two degrees of freedom vortex induced simulation of a circular cylinder using the solver pimpleFoam together with a morphing mesh approach. Unfortunately no work was found using this test case with the overset mesh method implemented in OpenFOAM.

Summing up, the purpose of this work is to compare the overset method and the morphing mesh method implemented in OpenFOAM with reference studies available in the literature. By using a two dimensional laminar configuration, the sources of errors are restricted to the numeric and the choice of the artificial boundaries. Assuming that the errors associated with imposing artificial boundaries conditions are not too big, one can directly make conclusions about the accuracy of methods used for the grid motion. Especially for the overset method an accurate estimation of the numerical error is required since the overset interpolation is known to not be mass conservative (see e.g. [3, 17]).

The paper is organized as follows: Section 2 describes the governing equations, Section 3 describes the test cases used for this validation study, Section 4 describes the meshes used, Section 5 gives a brief description of the numerical methods used, the results are exposed in Section 6 and the conclusion are drawn in Section 7.

2. Governing equations

2.1. **Fluid.** The equation of motion used in OpenFOAM for moving meshes are written in the Arbitrary-Euler-Lagrange (ALE) formulation. This formulation is one of the most popular if morphing meshes are used to describe the solid body deformation or displacement [18]. If the overset method is used, this formulation avoids to formulate the equation of motion in multiple frames of references [19]. For the derivation of the equation see [20, 21]. The continuity and momentum equations are in this form given by

$$\frac{\partial}{\partial t}\int \rho dV + \oint \rho \mathbf{n}\cdot(\mathbf{U}-\mathbf{U}_g)dS = 0, \tag{1}$$

$$\frac{\partial}{\partial t}\int \rho \mathbf{U} dV + \oint \rho \mathbf{n}\cdot(\mathbf{U}-\mathbf{U}_g)\mathbf{U} dS - \oint \rho\nu \mathbf{n}\cdot\nabla\mathbf{U} dS + \oint p\mathbf{n} dS = 0. \tag{2}$$

In the above equations $\mathbf{U}$ is the fluid velocity, p the pressure, ν the molecular viscosity and ρ the density. The only difference to the equation of motion in a fixed mesh is the introduction of a new variable, i.e. the grid velocity $\mathbf{U}_g$. In order to determine the grid velocity the space conservation law (SCL) has to be solved as (see also [2, 18])

$$\frac{\partial}{\partial t}\int dV - \oint \mathbf{n}\cdot\mathbf{U}_g dS = 0. \tag{3}$$

In order to not introduce additional mass conservation errors, the temporal discretisation of the SCL 3 should be the same as used in the other conservation equation (see [20, 2, 18]).

2.2. **Solid.** The equation of motion for the displacement $\mathbf{x_s}$ of the rigid bodies involved in the FSI problem, are derived from Newtons second law, as

$$m\ddot{\mathbf{x}}_\mathbf{s} = d\dot{\mathbf{x}}_\mathbf{s} + k\mathbf{x}_\mathbf{s} + \oint \mathbf{n} p dS + \oint \mathbf{n}\cdot\tau_\mathbf{vis} dS. \tag{4}$$

The above equation represent the usual spring mass damper system with additional two term which account for the influence of the fluid forces on the movement of the solid. $\tau_\mathbf{vis}$ is the viscose stress tensor. k represents the spring constant, m the mass of the solid and d is the damping constant.

2.3. **Mesh motion.** If the morping mesh approach is adopted, an additional equation is solved for the point displacement $\mathbf{p_d}$. Note that for the overset grid the topology of the mesh remains unchanged. The point displacement is added to the position of the points at the previous time step $\mathbf{p_0}$ to get the new points $\mathbf{p_n}$, as

$$\mathbf{p_n} = \mathbf{p_0} + \mathbf{p_d}. \tag{5}$$

In order to get a smooth transition from the displacement of the moving boundaries towards a usually zero displacement of the outer boundaries, a Laplacian equation is solved. In the version of OpenFOAM used in this work, an equation of the cell center displacement $\mathbf{c_d}$ is solved rather than one for the point displacement, given by

$$\nabla\bullet(\gamma\nabla\mathbf{c_d}) = 0. \tag{6}$$

The diffusivity γ is proportional to the inverse distance from the moving boundary. Once $\mathbf{c_d}$ is obtained, it is interpolated to the points of the cells by using an inverse distance interpolation to get $\mathbf{p_d}$.

3. Test cases

3.1. **One degree of freedom spring mass damper system.** Figure 1 shows the setup of the simulation of the one degree of freedom spring mass damper system: We have a closed square with a fluid initially at rest. Actually the fluid part does not play a role in this test case since we are interested only in the movement of the one degree of freedom spring-mass-damper system. In order to exclude any influence of the fluid force on the movement of the circular cylinder two possible approaches are possible: set the density ρ and the viscosity ν to zero (actually to a very small value to avoid possible divisions by zero) or set the test keyword in the dynamicMeshDict to yes. Setting the test keyword to yes deactivates the fluid forces. Both options deliver the same results for the present configuration. In this way the pressure force which acts normal to the solid body surface and the shear stress which acts parallel to it do not influence the motion of the cylinder.

The mass m is set to $m = 0.03575$ kg, the spring constant k of the linear spring is set to $k = 69.48$ N/m. Two different damping cases are considered. The first one is an undamped system. In the second case the damping constant d is set to $d = 0.0039$ Ns/m which corresponds to a weakly damped system. For undamped and weakly damped systems the oscillation induced by the fluid on the structure can have potentially disastrous effects. The spring has an initial extension of $z_0 = 0.0016$ m which corresponds to the diameter of the cylinder.

For this configuration we have an analytical solution which we can use to verify our solver, given by

$$z(t)/z_0 = e^{-0.5(d/m)t} cos(t\sqrt{k/m}). \tag{7}$$

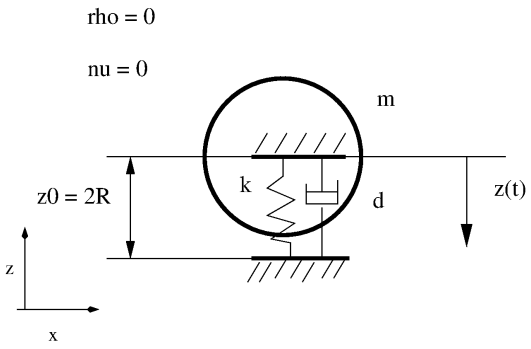

FIGURE 1. Setup of the simulation of the one degree of freedom spring mass damper system

3.2. **Inline oscillating cylinder.** Figure 2 shows the setup of the simulation for the inline oscillating cylinder: At the inflow a uniform velocity of $U_{inf} = 1m/s$ in x-direction is applied. The pressure is set to zero gradient at this boundary. At the top and bottom walls a slip boundary condition is applied. At the outlet the pressure is to be set equal to zero and for the velocity a zero gradient boundary condition is applied. The kinematic viscosity $\nu = 0.01m^2/s$ is set in order that the Reynolds number $Re = U_{inf}D/\nu$ based on the cylinder diameter $D = 1m$ is equal to $Re = 100$. For this Reynolds number the flow over a stationary cylinder is two dimensional. For this reason the flow is assumed to be two dimensional. This is imposed by using only one cell in span wise direction and setting both boundary conditions in this direction to the type empty. At the cylinder wall a no slip boundary condition is applied for the velocity and zero gradient for the pressure. The cylinder oscillates in x-direction with a prescribed sinosoidal motion: $x_c = Asin(2\pi f_c t) = Asin(\omega t)$. Four different frequencies are computed: $f_c = 0,\ 0.16,\ 0.33,\ 0.66\frac{1}{s}$. The amplitude is set to $A = 0.14$m. The main purpose of this test case was to check whether the increase of the lift at $f_c = 2f_{st}$ can be captured and if both techniques to simulate moving bodies deliver comparable results. The static frequency f_{st} is computed by performing a simulation around a fixed cylinder. The force signal in flow-normal direction is analyzed by fast Fourier transform (fft) and the frequency with the highest amplitude is used to compute f_{st}. The domain extends 20 D in upstream direction, 40 D in downstream direction and 20 D in both lateral direction for most simulation performed. This chosen domain size is in agreement with the settings used by other authors for inline oscillating cylinders: Leontini et al. [10] placed the outflow boundary at 50 D from the center of the cylinder. The location of the other boundaries are not mentioned. Liao et al. [6] used a domain which extends 50 D in stream wise direction and 70 D in lateral direction. Unfortunately, the coordinate of the cylinder center was not given by the author. The outer boundaries in the simulations performed by Do et al. [22] where located 10 D upstream, 40 D downstream and 12 D in lateral direction from the center of the cylinder. However, in order to confirm that the location of the outer boundaries have little influence on the solution, for the coarse overset mesh (see Section 4 for the description) and a frequency of $f_c = 3f_{st}$ four additional simulations are made: one where the upstream boundary was located at 40 D from the center of the cylinder and all other boundary location are kept unchanged (abbreviated as 40DUS), one where the downstream boundary was located at 80 D from the center of the cylinder and all other boundary location are kept unchanged (abbreviated as 80DDS), one where the lateral boundaries are located at 40 D from the center of the cylinder and all other boundary location are kept unchanged (abbreviated as 40DL) and a last one where the upstream boundary was located at 40 D, the downstream boundary at 80 D and the lateral boundaries at 40 D from the cylinder center (abbreviated as DD). Only the overset mesh is used for the domain size study since the influence of the domain boundaries should be similar for both mesh types investigated. Furthermore it is very easy for the overset mesh to ensure that the same grid is used in the overlapping regions of the five different meshes used for the domain size investigation.

3.3. **Vortex induced vibration of a cylinder.** Figure 3 shows the setup of the simulation were we analyze the vortex induced vibration of a circular cylinder: At the inflow a uniform velocity of $U_{inf} = 0.0656m/s$ in x-direction is applied. The pressure is set to zero gradient at this boundary. At the top

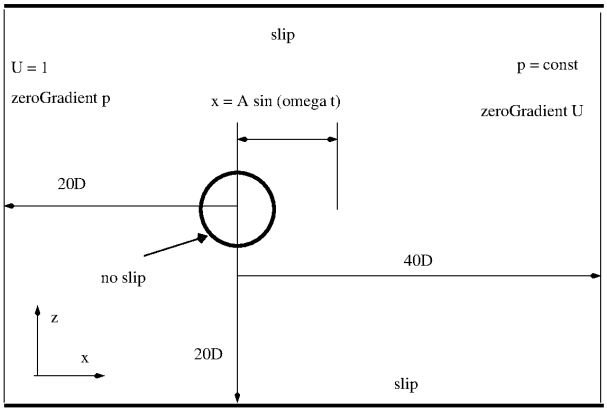

FIGURE 2. Setup of the simulation of the inline oscillating cylinder

and bottom walls a slip boundary condition is applied. At the outlet the pressure is to be set equal to zero and for the velocity a zero gradient boundary condition is applied. The kinematic viscosity $\nu = 1.05 \times 10^{-6} m^2/s$ is set in order that the Reynolds number $Re = U_{inf} D/\nu$ based on the cylinder diameter $D = 0.0016m$ is equal to $Re = 100$. For this Reynolds number the flow over a stationary cylinder is two dimensional. For this reason the flow is assumed to be two dimensional. This is imposed by using only one cell in span wise direction and setting both boundary conditions in this direction to the type empty. At the cylinder wall a no slip boundary condition is applied for the velocity and zero gradient for the pressure. The cylinder is free to oscillate in x- and y-direction. In this direction a linear spring restrain type is applied. The linear damping is set to zero in order to be comparable with the reference simulation of Singh and Mittal [23]. The domain extends 20 D in upstream direction, 40 D in downstream direction and 20 D in both lateral direction for most simulations. For this size of the computational domain, Prasanth and Mittal [24] found that the results are almost independent of the location of the boundaries. In order check the influence of the location of the domain boundaries, four additional simulation for the coarse overset mesh (see Section 4 for the description) and a $U^* = \frac{U_\infty}{f_n D}$ =5.5 are performed. The same domain sizes as described in Section 3.2 are used.

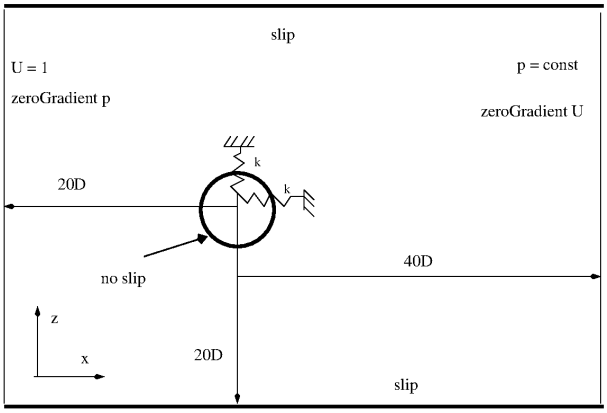

FIGURE 3. Setup of the vortex induced vibration simulation

Four different non dimensional velocities are computed: $U^* = \frac{U_\infty}{f_n D}$ =4, 4.8, 5 and 8.5. U_∞ is the incoming flow velocity and $f_n = \frac{\omega}{2\pi} = \frac{\sqrt{k/m}}{2\pi}$ is the natural frequency of the spring-mass system. The lowest and highest non-dimensional velocity correspond to cases in the work by Singh and Mattal [23], where the shedding frequency is not synchronized with the spring-mass system and therefore low amplitude oscillation of the mass occur. A U^* =4.8 correspond to the onset of synchronization with large amplitude oscillation ($y/D \approx 0.6$) in the reference experiment. A U^* =5.5 correspond to a region in the middle of the synchronization regime. Also for this case the reference experiment reported large amplitude oscillations. Having defined the diameter D of the cylinder, the incoming flow velocity U_∞ and the mass m = 0.03575 kg, after that one can determine the four different linear spring constants k =148.2, 102.97, 78.42 and 32.83 N/m for a non-dimensional velocity of U^* =4, 4.8, 5.5 and 8.5, respectively.

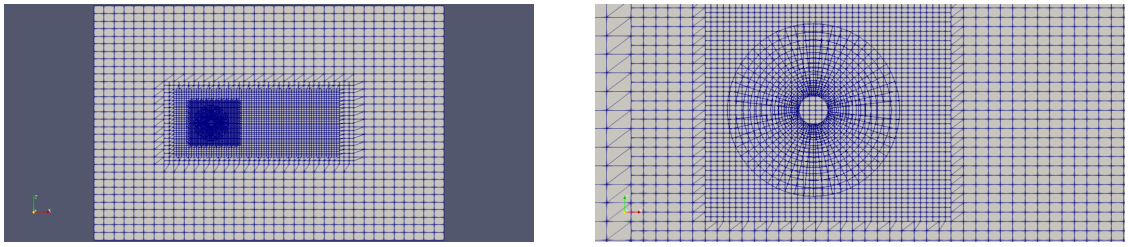

(A) Overview (B) Zoomed view

FIGURE 4. Mesh used for the overset method

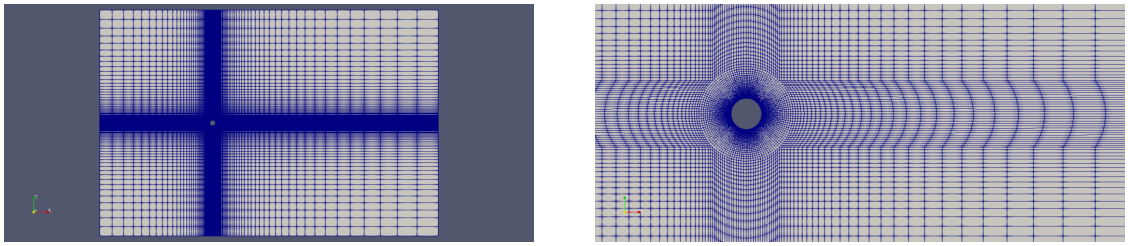

(A) Overview (B) Zoomed view

FIGURE 5. Mesh used for the morphing mesh method

The last non-dimensional parameter to match is the non-dimensional mass $m* = m/m_f = 4m/(\rho D^2 H)$. $H = 0.12$m is the height of the cylinder and m_f is the mass of the fluid occupied by the cylinder. In order to match this non-dimensional parameter the density of the cylinder is set to 14817 kg/m^3.

4. MESH GENERATION

In this section the meshes used for the simulations are described. Two types of meshes are used: one for the morphing mesh simulation and one for the overset simulations. Since the topology of the mesh is identical for all simulations and only the number of cells changes, the meshes employed are described only once.

The mesh used for the overset mesh simulation is shown in Figure 4. We can see that it is formed by the mesh surrounding the cylinder and the background mesh. The mesh surrounding the cylinder is generated by simply stretching the circular form of the cylinder outward. The background mesh consist of a rectangular block mesh with different refinement zones. In the outer part of the rectangle where the gradients of the flow field are smaller, a coarser mesh is used. Closer to the region surrounding the cylinder the mesh is finer. Note that when generating an overset mesh, it has to be paid attention that the cells at the intersection of the moving and the background mesh should have roughly the same size to minimize the interpolation errors.

Figure 5 shows the morphing mesh. It is generated using the utility blockMesh. Note that the dictionary for the generation of the mesh was taken online* and slightly modified in order to adopt it to the present test case. It is evident that the constitution of the mesh is much more complex compared to the overset mesh.

5. NUMERICAL METHODS

Both solvers used for the simulations (pimpleFoam for the morphing mesh method and overPimpleDyMFoam for the overset method) use the PIMPLE algorithm. It offers the possibility to use either the SIMPLE or the PISO algorithm to achieve an iterative pressure velocity coupling. The user can specify the number of outer iteration used to account for the non-linearity of the governing equations and the number of inner iterations which adjust the pressure in order to fulfill the mass conservation. For the details on the SIMPLE and the PISO algorithm the interested reader is referred to the book of Ferziger et al. [20]. For the details of the implementation in OpenFOAM the interested reader may have a look at the book of Moukalled et al. [25]. In the present study three outer and one inner iteration was used for

*https://curiosityfluids.com/2016/07/19/oscillating-cylinder-in-crossflow-pimpledymfoam/

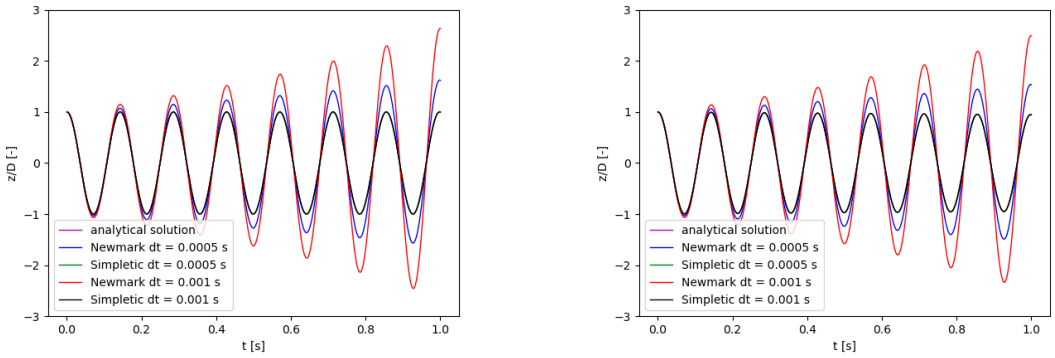

(A) Undamped (B) Damped

FIGURE 6. Response of the one degree of freedom mass-spring-damper system to an initial displacement for the overset mesh

all test cases. The divergence terms in the momentum equation are dicretized using a fourth-order cubic scheme. This scheme was found to be less diffusive compared to a linear scheme leading to higher lift and drag coefficients for a stationary cylinder. A second-order backward scheme was used for the temporal discretization. In order to study the influence of the disretization scheme for the divergence and the transient term on a moving cylinder, simulations with the first-order Euler scheme for the transient term and a second-order linear scheme for the divergence term are performance. A more detailed description is provided in the result section. For the overset method an inverse distance interpolation was used to interpolate the variables between the grids. Note that a fairly good description of the method implemented in OF1906 can be found in the work by Tisovska [26]. In order to advance the position of the solid body in time, two different methods are testes: The Symplectic methods developed by Dullweber et al. [27] and the Newmark method [28].

6. RESULTS

6.1. **One degree of freedom spring mass damper system.** Figure 6 shows the results obtained by the overset mesh. Two different time step sizes of dt = 0.0005 s and dt = 0.001 s are compared with each other. Furthermore two different method to integrate the ordinary differential equation are investigate: the Newmark method and the symplectic method. It has to be mentioned that the Newmark method for the overset method is explicit since the spring and damper force are not updated during the outer iterations of the pimple loop. In the Newmark method used for the morphing mesh approach the spring and damper forces are updated during the outer iterations of the pimple loop. For this reason it can be regarded as implicit. The symplectic method is explicit for both approaches compared here (spring and damper forces are kept constant within a time step). It is obvious that the Newmark method is unstable for both undamped and weakly damped system. The error decreases with decreasing time step. The symplectic method reproduces the analytical result exactly.

The results shown in Fig. 7 are obtained for the morphing mesh. Four different simulation are performed for the undamped (left) and damped case (right). The time step size was dt = 0.001 s. For one simulation the symplectic method was used to compute the evolution of the velocity and position of the solid. For the other three the Newmark method was used. For one simulation the acceleration of the solid body was not updated during the outer iterations (labeled as Newmark no outer correction). For the remaining simulations the acceleration of the solid body was updated during the two (labeled as Newmark 2 outer) and four (Newmark 4 outer) outer iterations. It is evident that for the cases where the Newmark method without updating the acceleration during the outer iteration is used, are not stable. The symplectic method is stable. The observations that the Newmark method is unstable if the acceleration is not updated during the outer iteration of the pimple loop agrees well with the findings achieved using the overset solver.

6.2. **Inline oscillating cylinder.** Before starting with the comparison between the overset mesh and the morphing mesh, the analysis of the influence of the domain size is summarized in Table 1. The coarse mesh is used for this study. A frequency of $\frac{f_c}{f_{st}} = 3$ is taken for this study since it is believed that the domain size should have the biggest influence on the results for this frequency since the drag

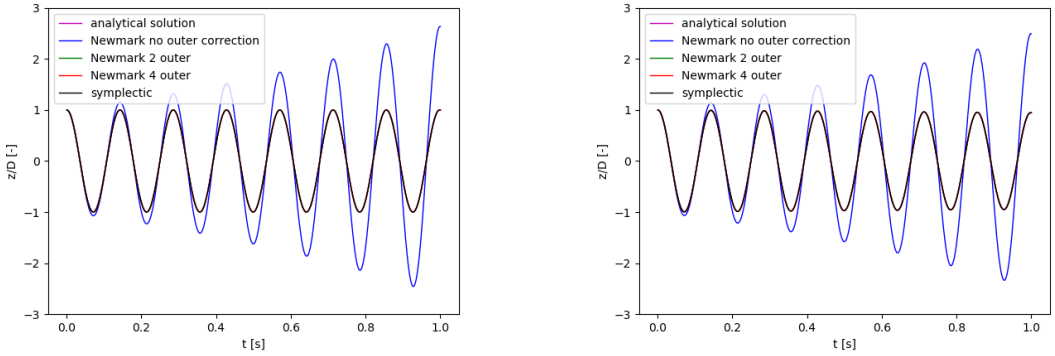

(A) Undamped (B) Damped

FIGURE 7. Response of the one degree of freedom mass-spring-damper system to an initial displacement for the morphing mesh

TABLE 1. Comparison of the Strouhal number, the mean drag coefficient $C_{d,mean}$ and the maximum lift coefficient $C_{l,max}$ for different domain sizes

	oc	oc 40DUS	oc 80DDS	oc 40DL	oc DD
St	0.157	0.157	0.157	0.157	0.157
$C_{d,mean}$	1.39	1.39	1.39	1.38	1.36
$C_{l,max}$	0.42	0.43	0.42	0.42	0.42

force is highest. It is evident that there are only small differences between the five different domain sizes analyzed when looking at integral quantities like the Strouhal number, the mean drag coefficient $C_{d,mean}$ and the maximum lift coefficient $C_{l,max}$. For this reason the smallest domain is sufficient to guarantee results which are independent of the domain size.

The comparison between overset mesh and the morphing mesh starts with a study on the influence of the discretization of the convective term and the time derivative in the momentum equation. For the purpose also the reduced frequency of $\frac{f_c}{f_{st}} = 3$ is taken. The coarse mesh is used. Three simulation for each mesh type are made: One with a fourth-order discretization for the convective term and a second-order discretization for the time derivative (abbreviated as t2d4), one with a fourth-order discretization for the convective term and a first-order discretization for the time derivative (abbreviated as t1d4) and one with a second-order discretization for the convective term and a second-order discretization for the time derivative (abbreviated as t2d2). The abbreviation oc stands for overset coarse and the abbreviation mc stands for morphing coarse. The comparison of the Strouhal number, the mean drag coefficient $C_{d,mean}$ and the maximum lift coefficient $C_{l,max}$ for different discretizations and mesh types is shown in Table 2. It is evident that the Strouhal number St is not affected by the chosen schemes. The mean drag coefficient $C_{d,mean}$ decreased for the overset mesh if a first-order Euler scheme is used instead of second-order backward. For the morphing mesh it remains unchanged. Changing the order of the discretisation of the convective scheme from fourth to second leads to a decrease in $C_{d,mean}$ for the overset mesh and increase for the morphing. The maximum lift coefficient $C_{l,max}$ increases for the overset mesh and remains unchanged for the morphing mesh changing the temporal discretisation from second to first order. Changing the convective scheme from fourth to second order leads to an increase of the maximum lift coefficients $C_{l,max}$ for the overset mesh and a slight reduction of the morphing mesh. The root mean square lift coefficient $C_{l,rms}$ is very little affected by the choice of the discretisation schemes. The reason why the morphing mesh and the overset mesh show different trends regarding the discretisation is not very clear. For the vortex-induced vibration case (see Table 6) the trend with respect to the discretisation schemes is however the same for the overset and the morphing mesh.

As advisable for every new simulation technique, we start with a small mesh convergence study. A mesh convergence study allows to guess the numerical errors (at least for laminar flows where no modeling errors are introduced) and to find a trade off between accuracy and time to solution. The results are presented in Table 3. The mesh study was made for two setups: the stationary cylinder and a reduced frequency of $\frac{f_c}{f_{st}} = 3$. The purpose was to check if the influence of the mesh resolution is different for

TABLE 2. Comparison of the Strouhal number, the mean drag coefficient $C_{d,mean}$, the maximum lift coefficient $C_{l,max}$ and the root mean square lift coefficient $C_{l,rms}$ for different discretizations and mesh types

	oc t2d4	mc t2d4	oc t1d4	mc t1d4	oc t2d2	mc t2d2
St	0.157	0.157	0.157	0.157	0.157	0.157
$C_{d,mean}$	1.39	1.32	1.31	1.32	1.34	1.34
$C_{l,max}$	0.42	0.46	0.46	0.47	0.45	0.44
$C_{l,rms}$	0.20	0.18	0.22	0.18	0.19	0.18

different oscillation frequencies. For the purpose of the mesh study, we analyzed three overset meshes: one with 17 300 (abbreviated as of), one with 13 300 (abbreviated as om) and one with 5 800 cells (abbreviated as oc). Tree morphing meshes one with 23 000 (abbreviated as mf), one with 12 700 (abbreviated as mm) and one with 7 400 cells (abbreviated as mc) are compared as well.

Table 3 shows the results of the mesh study. Reference simulations and experiments of a stationary cylinder are also included. The variables which are compared are the Strouhal number St, the mean drag coefficient $C_{d,mean}$ and the maximum lift coefficient $C_{l,max}$. The Strouhal number St is computed by analyzing the signal of the lift (force in z-direction). The time signal generated by the function object is interpolated to a equidistant time step size array of 10 000 points. An equidistant time spacing is required by the fft Python packages used. The last 3 000 points are used to compute the statistics in order to exclude the initial transient stage of the simulation. The Strouhal number is computed from the frequency with the highest amplitude. The simulations were run for 200 s. The signals of the last 60 s of the simulation are used to compute these three quantities. Since the purpose of this work is to evaluate the capability of OpenFOAM to simulate an oscillating cylinder, the first necessary step is to check the quality of the simulations for a fixed cylinder. It is evident that the agreement with the references is reasonable. The results of the overset mesh and the mesh generated with blockMesh are very close. This means that the overset interpolation does not deteriorate the quality of the results for this case and the errors introduced by the non-mass conservative interpolation is small. Regarding the analysis of the violation of the mass conservation see e.g. [3, 17] or Fig. 12. Interestingly the St number does not show any mesh influence. Regarding the overset mesh the paramters analyzed are close for all three meshes used. We see a slight increase of the maximum lift coefficient $C_{l,max}$ and the mean drag coefficient $C_{d,mean}$ remains almost unchanged. Regarding the morphing mesh, the lift coefficient $C_{l,max}$ slightly increases when the resolution is increased. The results shown are computed with a Python script which analyzes the forces computed around the cylinder. Of course the Python script is also provided within the downloadable files. Regarding the mesh study for $\frac{f_c}{f_{st}} = 3$, we can conclude that the solution still changes slightly. Both $C_{d,mean}$ and $C_{l,max}$ increase when changing from the morphing medium mesh to the morphing fine mesh. For the overset mesh $C_{d,mean}$ decreases from the medium to the fine mesh and $C_{l,max}$ remains unchanged. It is therefore recommended to use even finer meshes for both approaches in order to reach a mesh independent solution. To access the grid size necessary to have mesh independent results is not topic of the paper. The main purpose of this paper is to compare the results of the morphing mesh approach with the overset approach with similar number of cells.

Table 4 shows the comparison of the mean drag coefficient $C_{d,mean}$ and the maximum lift coefficient $C_{l,max}$ with other simulation (sim) for different oscillation frequencies f_c. For the present simulations also the Strouhal number computed with the frequency of the lift signal with the maximum amplitude is shown. It can see seen that both mean drag coefficient $C_{d,mean}$ and the maximum lift coefficient $C_{l,max}$ have a maximum at a frequency twice the shedding frequency of a fixed cylinder $f_c = 2f_{st}$. The difference between the morphing mesh and the overset mesh are marginal and the agreement with the reference simulations are reasonable. All simulation (the one of this work and also the reference simulations) report an almost tripling of the lift coefficient with respect to the stationary cylinder (see Table 3). The Strouhal number for $f_c = 2f_{st}$ is the same as for the stationary cylinder (see Table 3). That means that also the frequency lock in can be reproduced with both the overset and the morphing mesh. As shown for the previous study, the integral quantities (except the Strouhal number St) slightly vary between the coarse and the medium meshes used.

Figure 8 shows the comparison of the temporal evolution of drag coefficient in the last 60 s (it is the time span where the statistics shown in the tables are computed) of the simulation for the medium mesh. It is evident that for increasing frequency f_c the amplitude of the drag coefficient increases since the velocity at which the cylinder is displacing through the fluid increases. The results of the morphing mesh and the overset mesh are very close. The oscillatory part of the drag coefficient seems to by given

TABLE 3. Comparison of the mean drag coefficient $C_{d,mean}$ and the maximum lift coefficient $C_{l,max}$ with other simulation (sim) and experiments (exp) for different oscillation frequencies f_c different meshes

	overset			morphing		
	St	$C_{d,mean}$	$C_{l,max}$	St	$C_{d,mean}$	$C_{l,max}$
coarse $\frac{f_c}{f_{st}} = 0$	0.164	1.30	0.31	0.164	1.33	0.27
medium $\frac{f_c}{f_{st}} = 0$	0.164	1.33	0.33	0.164	1.33	0.30
fine $\frac{f_c}{f_{st}} = 0$	0.164	1.32	0.32	0.164	1.30	0.31
coarse $\frac{f_c}{f_{st}} = 3$	0.157	1.39	0.44	0.157	1.39	0.47
medium $\frac{f_c}{f_{st}} = 3$	0.157	1.43	0.50	0.157	1.36	0.50
fine $\frac{f_c}{f_{st}} = 3$	0.157	1.37	0.50	0.157	1.44	0.52
[6] (sim) $\frac{f_c}{f_{st}} = 0$		1.36	0.34			
[5] (sim) $\frac{f_c}{f_{st}} = 0$		1.42	0.32			
[29] (exp) $\frac{f_c}{f_{st}} = 0$	0.166					

TABLE 4. Comparison of the mean drag coefficient $C_{d,mean}$ and the maximum lift coefficient $C_{l,max}$ with other simulation (sim) for different oscillation frequencies f_c

	overset			morphing		
	St	$C_{d,mean}$	$C_{l,max}$	St	$C_{d,mean}$	$C_{l,max}$
coarse $\frac{f_c}{f_{st}} = 1$	0.157	1.36	0.45	0.157	1.36	0.40
coarse $\frac{f_c}{f_{st}} = 2$	0.164	1.52	0.93	0.164	1.62	0.90
coarse $\frac{f_c}{f_{st}} = 3$	0.157	1.39	0.44	0.157	1.39	0.47
medium $\frac{f_c}{f_{st}} = 1$	0.157	1.37	0.46	0.164	1.36	0.42
medium $\frac{f_c}{f_{st}} = 2$	0.164	1.57	0.92	0.164	1.58	0.91
medium $\frac{f_c}{f_{st}} = 3$	0.157	1.43	0.50	0.157	1.36	0.50
[6] (sim) $\frac{f_c}{f_{st}} = 2$		1.71	0.95			
[5] (sim) $\frac{f_c}{f_{st}} = 2$		1.70	0.97			

by the movement of the cylinder. This is clearly visible by the functional evolution of C_d. The lower the frequency of the moving cylinder, the lower is also the frequency of the drag coefficient. There is no phase shift visible between the overset mesh and the morphing mesh. For both approaches the functional evolution of the position of the cylinder is the same. The drag force can be divided into friction and pressure contribution. Actually the pressure contribution can be divided into pressure difference between front and rear part of the cylinder as a result of the wake and a contribution resulting from the acceleration of the fluid induced by the acceleration of the cylinder (it's called added mass effect). Both contribution are influenced by the resolution. The grid close to the cylinder is very similar for the overset mesh and the morphing mesh. This can partially explain the not visible differences. The marginal difference between morphing and overset mesh can be seen also by the mean drag coefficient displayed in Table 4.

Figure 9 shows the comparison of the temporal evolution of lift coefficient during the initial transient stage. The temporal evolution of the lift coefficient is similar for both simulation approaches except for a frequency of $f_c = 3f_{st}$. For this frequency the initial transient stage of the overset mesh is much shorter compared to the morphing mesh. The reason is not clear. A cautious guess is that the numerical errors of the overset mesh lead to a faster destabilization of the initial steady solution. Figure 10 shows the comparison of the temporal evolution of lift coefficient during the fully developed stage of the simulation. It is obvious that for a frequency of $f_c = 2f_{st}$ the amplitude of the lift coefficient is highest. Again the results of the morphing mesh and the overset mesh are very similar. From the signals it is also evident, that the higher frequencies content increases with f_c. Figure 11 shows the amplitude spectrum of the lift coefficient for the four oscillation frequencies f_c analyzed using both mesh types. The results of both mesh types are again very similar. The amount of peaks increase with increasing f_c. Note that the amplitudes of the lift coefficient C_l calculated by the fft of Python are very close to the one recorded (compare Fig. 11 with Fig. 10) demonstrating the usefulness of the provided Python scripts to retrieve the frequencies with the highest amplitudes.

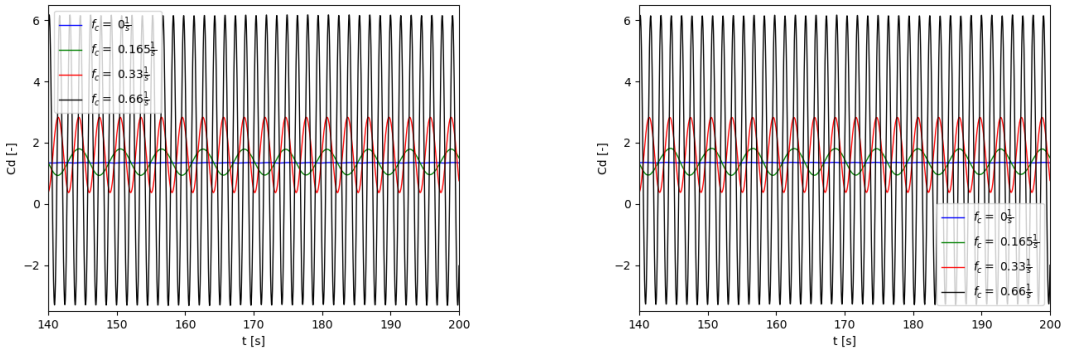

(A) Morphing mesh (B) Overset mesh

FIGURE 8. Comparison of the drag coefficient of the morphing mesh and overset mesh

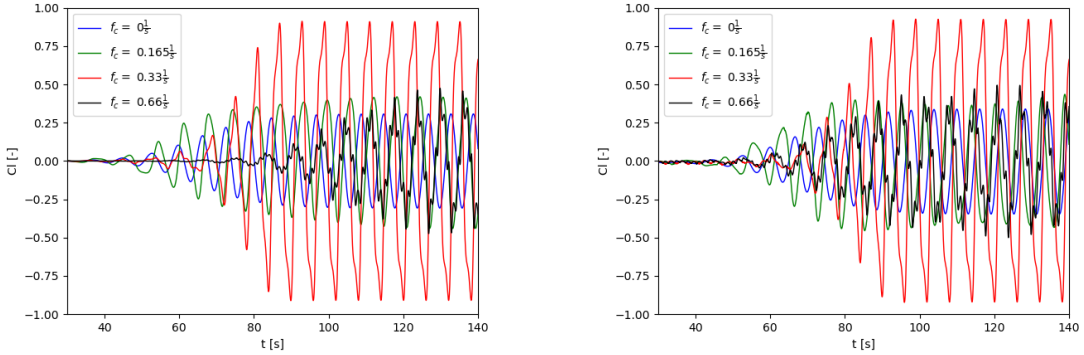

(A) Morphing mesh (B) Overset mesh

FIGURE 9. Comparison of the lift coefficient of the morphing mesh and overset mesh at the beginning of the simulation

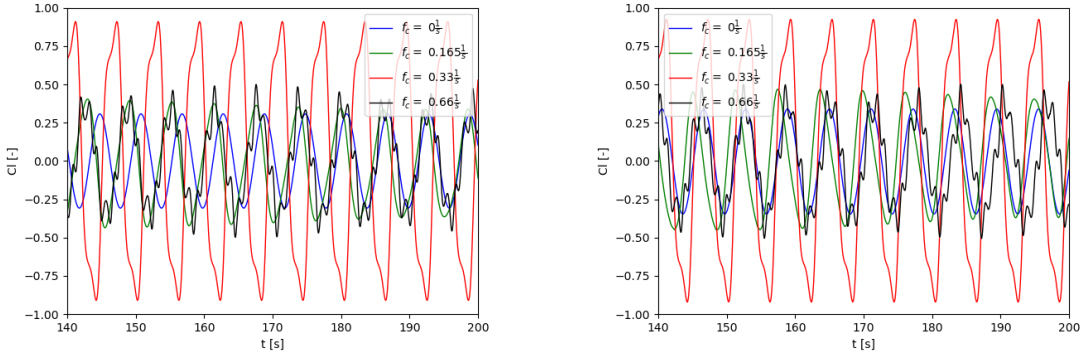

(A) Morphing mesh (B) Overset mesh

FIGURE 10. Comparison of the lift coefficient of the morphing mesh and overset mesh for the developed phase

A final remark should be made regarding the computational time. For the fixed cylinder and the case with an oscillation frequency $f_c = 0.16$, the simulations with the morphing mesh are much faster. For increasing frequency however, the maximum Courant number Co_{max} had to be decreased from 0.75 for $f_c = 0.16$ to $Co_{max} = 0.5$ for $f_c = 0.33$ and $Co_{max} = 0.25$ for $f_c = 0.66$ for the morphing mesh. The

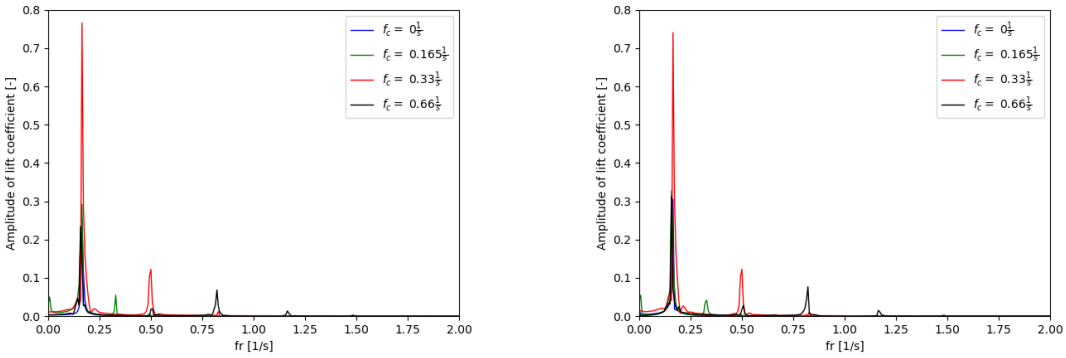

(A) Morphing mesh (B) Overset mesh

FIGURE 11. Comparison of the amplitude spectrum of lift for the morphing mesh and overset mesh

TABLE 5. Comparison of the St number, the r.m.s drag coefficient $C_{d,rms}$, the r.m.s lift coefficient $C_{l,rms}$, the r.m.s of the x-displacement x_{rms}/D and the maximum z-displacement z_{max}/D for different domain sizes

	oc	oc 40DUS	oc 80DDS	oc 40DL	oc DD
St	0.175	0.175	0.175	0.175	0.175
$C_{d,rms}$	0.36	0.35	0.35	0.35	0.34
$C_{l,rms}$	0.46	0.48	0.46	0.49	0.51
z_{max}/D	0.57	0.57	0.57	0.56	0.57
x_{rms}/D	0.01	0.009	0.008	0.009	0.008

purpose was to avoid nonphysical pressure peaks which occurred for higher Co_{max}. For this reason the simulation time for the cases with the highest frequency was comparable between both mesh types. For the overset mesh the maximum Courant number $Co_{max} = 0.75$ was the same for all frequencies and the coarse and the medium mesh. For the fine mesh however, a Courant number of $Co_{max} = 0.5$ had to be used to avoid nonphysical high amplitude and high frequency oscillation in the lift and drag signal. The reason for this is not really clear. According to Benjamin et al. [30] the mesh Courant number for moving meshes should be of order unity to guarantee high quality results. For the highest frequency $f_c = 0.66$ we get a maximum velocity of the cylinder of 0.58 m/s. The smallest cell size in the region where the background mesh and the mesh around the cylinder overlap is $\Delta x = 0.125$ m. With these quantities we get the time needed for the mesh to cover a distance equal to the smallest cell size of 0.21 s. The typical time step size used in the simulation is of the order of 0.01 s and hence much smaller than the time required for the moving mesh to cross a cell of the background mesh.

6.3. **Vortex induced vibration of a cylinder.** Before starting with the comparison between the overset mesh and the morphing mesh, the analysis of the influence of the domain size is summarized in Table 5. It is evident that the St number is independent of the size of the domains analyzed. We observe a small reduction of the r.m.s. drag coefficient $C_{d,rms}$ and small increase of the r.m.s lift coefficient $C_{l,rms}$ if the domain size is doubled. The maximum z-displacement z_{max}/D remains unchanged between the difference position of the domain boundaries. The maximum z-displacement z_{max}/D is reduced slightly if the domain size is doubled. Since the changes of these integral quantities are very small, the smallest domain size is used in order to save computational time.

The comparison between the overset mesh and the morphing mesh starts as for the forced oscillation case with a study on the influence of the discretization of the convective term and the time derivative in the momentum equation. For the purpose also the reduced velocity of $U^* = 5.5$ is taken. The coarse mesh is used. Three simulations for each mesh type are made: One with a fourth-order discretization for the convective term and a second-order discretization for the time derivative (abbreviated as t2d4), one with a fourth-order discretization for the convective term and a first-order discretization for the time derivative (abbreviated as t1d4) and one with a second-order discretization for the convective term and a second-order discretization for the time derivative (abbreviated as t2d2). Table 6 shows the comparison

TABLE 6. Comparison of the Strouhal number, the root mean square drag coefficient $C_{d,rms}$ and the root mean square lift coefficient $C_{l,rms}$, the root mean square of the x-displacement x_{rms}/D and the maximum z-displacement z_{max}/D for different discretizations and mesh types

	oc t2d4	mc t2d4	oc t1d4	mc t1d4	oc t2d2	mc t2d2
St	0.175	0.177	0.175	0.177	0.175	0.177
$C_{d,rms}$	0.36	0.34	0.36	0.34	0.37	0.37
$C_{l,rms}$	0.46	0.32	0.53	0.38	0.45	0.32
z_{max}/D	0.57	0.55	0.56	0.56	0.57	0.56
x_{rms}/D	0.01	0.008	0.01	0.009	0.01	0.01

TABLE 7. Mesh comparison study for $U^* = 5.5$: Comparison of the St number, the r.m.s drag coefficient $C_{d,rms}$, the r.m.s lift coefficient $C_{l,rms}$, the r.m.s of the x-displacement x_{rms}/D and the maximum z-displacement z_{max}/D

	of	om	oc	mf	m. m.	mm	[23]
St	0.180	0.174	0.173	0.179	0.181	0.184	0.179
$C_{d,rms}$	0.35	0.35	0.35	0.34	0.34	0.34	0.33
$C_{l,rms}$	0.47	0.45	0.44	0.31	0.29	0.29	0.24
z_{max}	0.57	0.57	0.57	0.55	0.55	0.55	0.53
x_{rms}	0.006	0.006	0.006	0.0057	0.0057	0.0059	0.0056

of the Strouhal number, the root mean square drag coefficient $C_{d,rms}$ and the root mean square lift coefficient $C_{l,rms}$, the root mean square of the x-displacement x_{rms}/D and the maximum z-displacement z_{max}/D for different discretizations and mesh types. It is evident that the Strouhal number St is not affected by the discretisation schemes. The r.m.s drag coefficient $C_{d,rms}$ increases when switching from a fourth-order to a second-order convective scheme. The temporal discretisation has little influence on this quantity. The trend is the same for the overset and the morphing mesh. The r.m.s. lift coefficient $C_{l,rms}$ is almost not affected by the chosen convective scheme. Using the first-order Euler scheme instead of the second-order backward scheme increases the $C_{l,rms}$. Again the trend is the same for the overset and the morphing mesh. The root mean square of the x-displacement x_{rms}/D and the maximum z-displacement z_{max}/D are not affected by the schemes chosen.

As advisable for every new simulation technique, we start with a small mesh convergence study. For this purpose we analyzed three overset meshes: one with 17 300 (abbreviated as of), one with 13 300 (abbreviated as om) and one with 5 800 cells (abbreviated as oc). Three morphing meshes one with 23 000 (abbreviated as mf), one with 12 700 (abbreviated as mm) and one with 7 400 cells (abbreviated as mc) are compared as well.

Table 7 shows the mesh comparison study for a $U^* = 5.5$. The results of the fine, medium and the coarse mesh are compared to reference simulations. The table shows the St number $St = fD/U$, the r.m.s drag coefficient $C_{d,rms}$, the r.m.s lift coefficient $C_{l,rms}$, the r.m.s of the x-displacement x_{rms}/D and the maximum z-displacement z_{max}/D. The shedding frequency f is calculated using the time signal of the lift force. The time signal generated by the function object is interpolated to a equidistant time step size array of 3 000 points. An equidistant time spacing is required by the fft Python packages used. The last 1 000 points are used to compute all statistics shown in Table 7 and Table 8 in order to exclude the initial transient stage of the simulation. The results are compared with the simulations of Singh and Mittal [23]. From these integral coefficients it is evident that no big differences are visible between the coarse, medium and fine overset mesh and the coarse, medium and fine morphing mesh. For this reason all further computations are made with the coarse version of both meshes in order to save computational resources. The agreement with the reference simulation is reasonable.

Since it is known that the overset methodology is not mass conservative, Figure 12 shows the normalized difference $\dot{m}_n = (\dot{m}_{in} - \dot{m}_{ou})/\dot{m}_{in} * 100$ of the mass flow rate at the inlet $\dot{m}_{in}$ and the mass flow rate at the outlet $\dot{m}_{ou}$. Note that the normalized mass flow difference is shown in percent. It is evident that there exists a small imbalance between the flow rate at the inlet and the outlet. It decreases for a finer mesh.

Table 8 compares the St number, the r.m.s drag coefficient $C_{d,rms}$, the r.m.s lift coefficient $C_{l,rms}$, the r.m.s of the x-displacement x_{rms}/D and the maximum z-displacement z_{max}/D for different U^* with the simulations of Singh and Mittal [23]. It is evident that the best agreement with the reference simulation

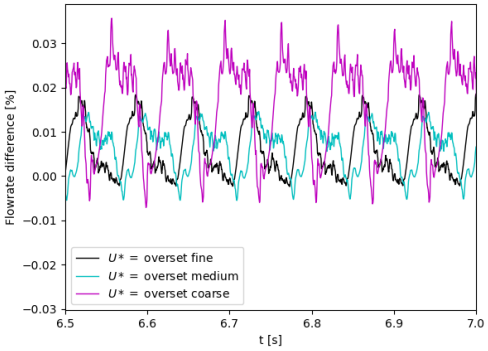

FIGURE 12. Normalized flow rate difference in percent of the three overset meshes used.

TABLE 8. Comparison of the St number, the r.m.s drag coefficient $C_{d,rms}$, the r.m.s lift coefficient $C_{l,rms}$, the r.m.s of the x-displacement x_{rms}/D and the maximum z-displacement z_{max}/D for different U^*

	St	$C_{d,rms}$	$C_{l,rms}$	z_{max}/D	x_{rms}/D
overset $U^* = 4$	0.156	0.006	0.20	0.012	0.002
morping $U^* = 4$	0.167	0.0059	0.25	0.016	0.001
[23] $U^* = 4$	0.172	0.0	0.30	0.028	0.00019
overset $U^* = 4.8$	0.156	0.0047	0.24	0.031	0.001
morping $U^* = 4.8$	0.186	0.100	0.65	0.268	0.003
[23] $U^* = 4.8$	0.198	0.47	0.63	0.56	0.0063
overset $U^* = 5.5$	0.175	0.36	0.46	0.57	0.01
morping $U^* = 5.5$	0.177	0.34	0.32	0.55	0.008
[23] $U^* = 5.5$	0.179	0.33	0.24	0.53	0.0056
overset $U^* = 8.5$	0.146	0.023	0.10	0.11	0.002
morping $U^* = 8.5$	0.156	0.013	0.15	0.065	0.001
[23] $U^* = 8.5$	0.161	0.0	0.18	0.037	0.00023

is obtained for the morphing mesh. For $U^* = 4.8$ where Singh and Mittal [23] obtained already a locked in state, the overset mesh simulation reports only small oscillation and the morphing mesh simulation seems to be in a transitional regime right before the onset of lock in (see Fig. 14 displaying the evolution of the z-displacement). For the highest non-dimensional velocity $U^* = 8.5$ the overset mesh predicts higher oscillations compared with Singh and Mittal [23] and the morphing mesh. It has be be said that this U^* lays very close to the end of the lock in region reported by Singh and Mittal [23]. It seems that the boarders of the lock in region obtained with the overset mesh are shifted towards higher U^* compared with the morphing mesh and the reference simulation. This is also confirmed by looking at the r.m.s lift coefficient $C_{l,rms}$ at a $U^* = 5.5$ for the overset mesh. The values are much higher compared with the morphing mesh and the results of Singh and Mittal [23]. Singh and Mittal [23] reported a drastic increase of $C_{l,rms}$ at $U^* = 4.7$ (when lock in occurs). The maximum of $C_{l,rms}$ is also at $U^* = 4.7$. After that $C_{l,rms}$ monotonically decreases with U^*. The displacements also decrease monotonically after $U^* = 4.7$ but not so fast as the lift. This means that if for the overset mesh the onset of lock in is predicted at higher U^* respect to the reference, it is in line with this observation that in the lock in regime $C_{l,rms}$ is higher for the overset mesh compared with the reference.

Figure 13 compares the work done from the start of the simulation (t = 0) until the time t by the fluid on the cylinder for the two mesh types and the four non-dimensional velocities analyzed. It is calculated as follows:

$$W(t) = \int_0^t F_z(\tau) v_z(\tau) d\tau \tag{8}$$

F_z is the force in the z-direction exerted by the fluid on the cylinder and v_z is the z-velocity. According to Mittal et al. [14] and Morse and Williamson [31], the main mechanisms which lead to large amplitude oscillation is a positive energy transfer (or work done) over an oscillation cycle from the fluid to the

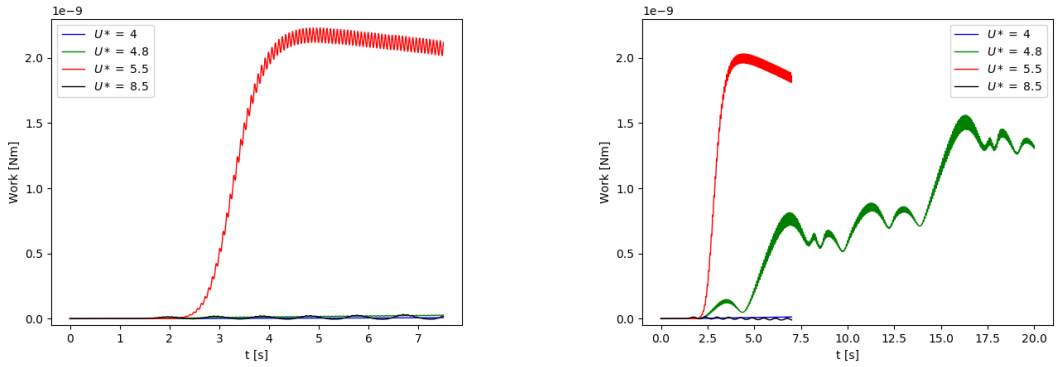

(A) Overset mesh (B) Morphing mesh

FIGURE 13. Work done by the fluid on the cylinder

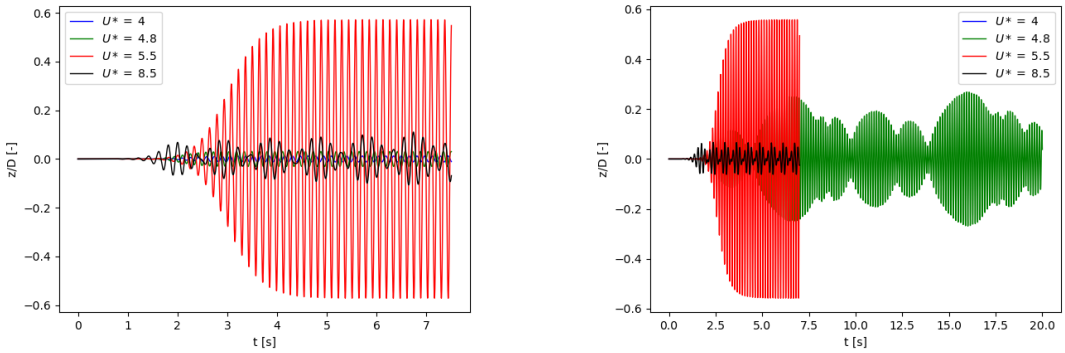

(A) Overset mesh (B) Morphing mesh

FIGURE 14. Displacement in z-direction for different U^* and the two mesh types

oscillator. In order to check if this mechanisms can be found also in the present study, the work done by the fluid is plotted in figure 13. It is evident that for the cases with large oscillations in the z-direction the work done experiences a sharp increase and after that it remains constant. The large work done by the fluid is necessary to increase the amplitude of the displacement. After that a mean steady state is reached where the work done by the fluid over an oscillation cycle has to be zero for the present simulations without structural damping [14]. For this reason the total work done by the fluid on the oscillator converges to a constant value.

Figure 14 shows the temporal evolution of the z-displacement of the cylinder for the overset mesh and the morphing mesh. It is evident that the maximum displacement is observed for U^* =5.5 for both meshes. For $U^* = 4$ both mesh types show small oscillations. A remarkable difference between the two mesh types is observed for $U^* = 4.8$: While for the overset mesh the amplitude of the oscillations is still small as in the pre-lock in regime, for the morphing mesh we can observed an intermittent behavior as observed by Prasanth and Mittal [24] in the small transition region before lock in occurs. For $U^* = 8.5$ the amplitude of the overset mesh is higher compared to the morphing mesh.

Figure 15 shows the temporal evolution of the x-coordinate of the cylinder for the overset mesh and the morphing mesh. We can see that the two approaches deliver slightly different equilibrium position of the x-coordinate. The oscillations around the equilibrium position are very small for both approaches. The maximum fluctuation of the x-coordinate are observed for both mesh types for $U^* = 5.5$. The magnitude is less than 5% of the cylinder for this case. For the reduced velocities $U^* = 5.5$ and 8.5 a slightly shorter initial transient phase can be observed for the morphing mesh approach compared to the overset mesh. For the other two reduced velocities analyzed no visible difference in the duration of the initial transient phase can be seen.

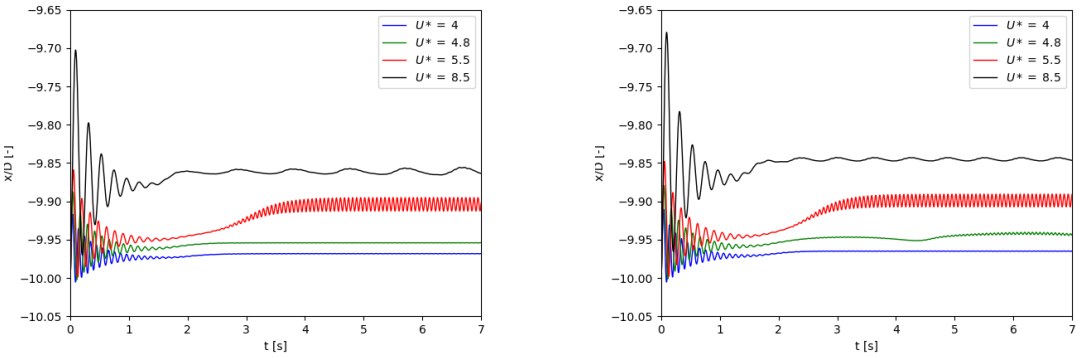

(A) Overset mesh (B) Morphing mesh

FIGURE 15. Displacement in x-coordinate for different U^* and the two mesh types

Figure 16 shows snapshots of z-vorticity for the overset and morphing mesh for $U^* = 4$, $U^* = 5.5$ and $U^* = 8.5$. For the first two non-dimensional velocities the shedding modes are different. For the lower non-dimensional velocity the shedding mode is similar to a stationary cylinder: Two single vortecies are shed per cycle from the cylinder. This shedding mode is called 2P mode which is also observed by Singh and Mittal [23] and Prasant and Mittal [24] in the low amplitude case. For the high amplitude oscillations case these two vortecies merge giving rise to the C(2P) mode also observed by Singh and Mittal [23] and Prasant and Mittal [24]. The flow pictures obtained with the overset mesh and the morphing mesh are very similar for these two U^*. For $U^* = 8.5$, where the fluid flow is outside the lock in regime, the flow picture is again similar to a stationary cylinder resulting in a 2P mode. The same is observed also by Singh and Mittal [23] and Prasant and Mittal [24].

7. CONCLUSION

In this work we analyzed the behavior of the overset method and the morphing mesh method with the help of a two-dimensional cylinder configuration. First the solution obtained with the six-degree of freedom solver was compared with an analytical solution of spring-mass-damper system. As next step the complexity of the case analyzed was increased and the inline oscillation of a cylinder was simulated. Finally the vortex induced oscillation was tackled. The purpose of increasing the complexity of the test cases step by step is to isolate potential hurdles. Furthermore it is easier to understand a complex configuration if beforehand easier problems are analyzed and understood.

Regarding the one degree of freedom spring mass damper system we can draw following conclusions:

- It is very useful to verify numerical methods with analytical solutions. From my experience as model developer and programmer one can get rid of the majority of bugs and errors in the settings if one compares the results of the simulation with an analytical solution where one exactly knows the outcome.
- If the overset mesh is used, it is recommended to use the symplectic solver. The Newmark is unstable for a undamped and weakly damped system.
- If the morphing mesh is used, it is recommended to update the acceleration of the solid body during the outer iterations if the Newmark method is used.

Regarding the inline oscillation cylinder we can draw following conclusions:

- The results of the overset mesh are very similar to the one obtained with the morphing mesh.
- The maximum of the lift occurs at twice the shedding frequency of the stationary cylinder. This is in line with the findings of other simulations and experiments.
- Frequency lock in at $f_c = 2f_{st}$ can be reproduced with both overset and morphing mesh.
- A mesh study has revealed that for an oscillating cylinder more grid points are required to reach a mesh independent result compared to a fixed cylinder.

Regarding the vortex induced oscillation we can draw following conclusions:

- Both overset mesh and morphing mesh can predict the large amplitude oscillations of the cylinder in the lock in regime. Outside this regime (for lower and higher values of non-dimensional velocity U^*) the reported amplitudes of the structural oscillations are low. Inside the lock in regime the

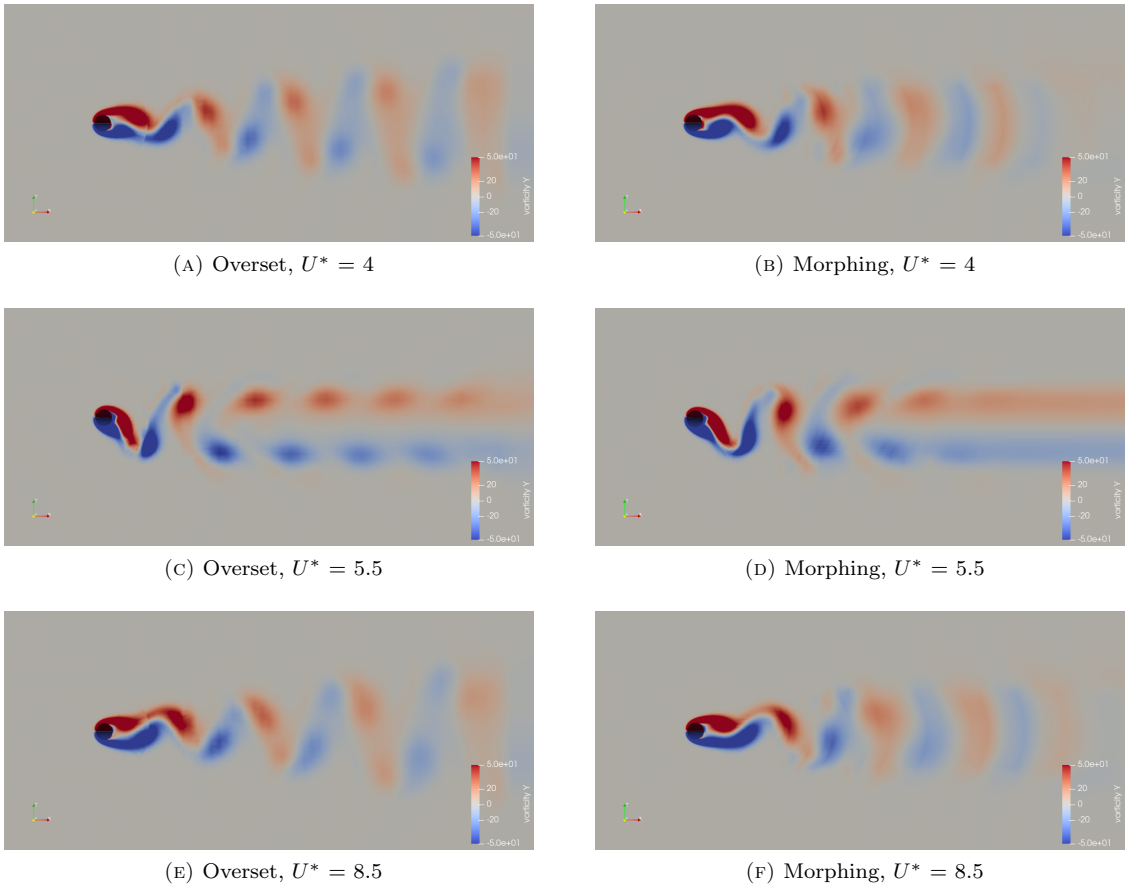

(A) Overset, $U^* = 4$ (B) Morphing, $U^* = 4$

(C) Overset, $U^* = 5.5$ (D) Morphing, $U^* = 5.5$

(E) Overset, $U^* = 8.5$ (F) Morphing, $U^* = 8.5$

FIGURE 16. Snapshots of z-vorticity for the overset and morphing mesh for $U^* = 4$, $U^* = 5.5$ and $U^* = 8.5$

two single vortices shed per cycle merge resulting in the so called C(2P) mode. Outside the lock in regime the two single vortices are maintained also further downstream. The same observations are made also by Singh and Mittal [23] and Prasant and Mittal [24].

- It seems that the boarders of the lock in region obtainable with the overset mesh with the settings used in this work are shifted towards higher U^* compared with the morphing mesh and the reference simulation.
- For the current settings the morphing mesh is up to two times faster compared with the overset mesh for similar number of cells. The reason is probably that the pressure solver requires more iterations for the overset mesh compared to the morphing mesh. For this reason it is better to use the former if the movements of the structure are not too large to deteriorate the mesh quality. Note also that all cases are run in serial. The performance analysis should be done also for a parallel run. This is not in the scope of the current work.
- The work done by the fluid on the cylinder is highest for the cases with the highest amplitude oscillations.

Author Contributions: Conceptualisation, M.A.; methodology, M.A.; software, M.A; validation, M.A.; formal analysis, M.A.; investigation, M.A.; resources, M.A.; data curation, M.A.; writing—original draft preparation, M.A.; writing—review and editing, M.A.; visualisation, M.A.; supervision, M.A.; All authors have read and agreed to the published version of the manuscript.

REFERENCES

[1] E. H. Dowell and K. C. Hall, "Modeling of fluid-structure interaction," *Annual review of fluid mechanics*, vol. 33, no. 1, pp. 445–490, 2001.

[2] H. Jasak, "Dynamic mesh handling in openfoam," in *47th AIAA aerospace sciences meeting including the new horizons forum and aerospace exposition*, 2009, p. 341.

[3] S. Völkner, J. Brunswig, and T. Rung, "Analysis of non-conservative interpolation techniques in overset grid finite-volume methods," *Computers & Fluids*, vol. 148, pp. 39–55, 2017.

[4] H. Gopalan, R. Jaiman, and D. D. Chandar, "Flow past tandem circular cylinders at high reynolds numbers using overset grids in openfoam," in *53rd AIAA Aerospace Sciences Meeting*, 2015, p. 0315.
[5] S.-W. Su, M.-C. Lai, and C.-A. Lin, "An immersed boundary technique for simulating complex flows with rigid boundary," *Computers & fluids*, vol. 36, no. 2, pp. 313–324, 2007.
[6] C.-C. Liao, Y.-W. Chang, C.-A. Lin, and J. McDonough, "Simulating flows with moving rigid boundary using immersed-boundary method," *Computers & Fluids*, vol. 39, no. 1, pp. 152–167, 2010.
[7] D. D. Chandar, B. Boppana, and V. Kumar, "A comparative study of different overset grid solvers between openfoam, starccm+ and ansys-fluent," in *2018 AIAA Aerospace Sciences Meeting*, 2018, p. 1564.
[8] O. M. Griffin and M. Hall, "Vortex shedding lock-on and flow control in bluff body wakes," 1991.
[9] Y. Tanida, A. Okajima, and Y. Watanabe, "Stability of a circular cylinder oscillating in uniform flow or in a wake," *Journal of Fluid Mechanics*, vol. 61, no. 4, pp. 769–784, 1973.
[10] J. S. Leontini, D. L. Jacono, and M. C. Thompson, "A numerical study of an inline oscillating cylinder in a free stream," *Journal of Fluid Mechanics*, vol. 688, pp. 551–568, 2011.
[11] L. Shen, E.-S. Chan, and P. Lin, "Calculation of hydrodynamic forces acting on a submerged moving object using immersed boundary method," *Computers & Fluids*, vol. 38, no. 3, pp. 691–702, 2009.
[12] M. Pomarede, E. Longatte, and J.-F. o. Sigrist, "Benchmark of numerical codes for coupled csd/cfd computations on an elementary vortex induced vibration problem," in *ASME Pressure Vessels and Piping Conference*, vol. 43673, 2009, pp. 537–546.
[13] C. Williamson and R. Govardhan, "Vortex-induced vibrations," *Annu. Rev. Fluid Mech.*, vol. 36, pp. 413–455, 2004.
[14] S. Mittal *et al.*, "Lock-in in vortex-induced vibration," *Journal of Fluid Mechanics*, vol. 794, pp. 565–594, 2016.
[15] D. Sabino, D. Fabre, J. Leontini, and D. L. Jacono, "Vortex-induced vibration prediction via an impedance criterion," *Journal of Fluid Mechanics*, vol. 890, 2020.
[16] P. D. d. S. Conceição, "Numerical simulation of two-degree-of-freedom vortex induced vibration in a circular cylinder with openfoam," Ph.D. dissertation, 2016.
[17] S. Lemaire, G. Vaz, M. Deij-van Rijswijk, and S. R. Turnock, "On the accuracy, robustness and performance of high order interpolation schemes for the overset method on unstructured grids," *International Journal for Numerical Methods in Fluids*, 2021.
[18] M. Breuer, G. De Nayer, M. Münsch, T. Gallinger, and R. Wüchner, "Fluid–structure interaction using a partitioned semi-implicit predictor–corrector coupling scheme for the application of large-eddy simulation," *Journal of Fluids and Structures*, vol. 29, pp. 107–130, 2012.
[19] W. J. Horne and K. Mahesh, "A massively-parallel, unstructured overset method to simulate moving bodies in turbulent flows," *Journal of Computational Physics*, vol. 397, p. 108790, 2019.
[20] J. H. Ferziger, M. Perić, and R. L. Street, *Computational methods for fluid dynamics*. Springer, 2002, vol. 3.
[21] M. Buchmayr, *Development of Fully Implicit Block Coupled Solvers for Incompressible Transient Flows*. TU-Graz, 2014.
[22] T. Do, L. Chen, and J. Tu, "Numerical simulations of flows over a forced oscillating cylinder," 2007.
[23] S. Singh and S. Mittal, "Vortex-induced oscillations at low reynolds numbers: hysteresis and vortex-shedding modes," *Journal of Fluids and Structures*, vol. 20, no. 8, pp. 1085–1104, 2005.
[24] T. Prasanth and S. Mittal, "Vortex-induced vibrations of a circular cylinder at low reynolds numbers," *Journal of Fluid Mechanics*, vol. 594, p. 463, 2008.
[25] F. Moukalled, L. Mangani, M. Darwish *et al.*, *The finite volume method in computational fluid dynamics*. Springer, 2016, vol. 113.
[26] P. Tisovska, "Description of the overset mesh approach in esi version of openfoam," *Proceedings of the CFD with OpenSource Software; Nilsson, H., Ed*, 2019.
[27] A. Dullweber, B. Leimkuhler, and R. McLachlan, "Symplectic splitting methods for rigid body molecular dynamics," *The Journal of chemical physics*, vol. 107, no. 15, pp. 5840–5851, 1997.
[28] N. M. Newmark, "A method of computation for structural dynamics," *Journal of the engineering mechanics division*, vol. 85, no. 3, pp. 67–94, 1959.
[29] C. H. Williamson, "Vortex dynamics in the cylinder wake," *Annual review of fluid mechanics*, vol. 28, no. 1, pp. 477–539, 1996.
[30] T. K. J. Benjamin, H. Hesse, and P. C. Wang, "Wing-tail interaction under forced harmonic pitch," in *AIAA AVIATION 2021 FORUM*, 2021, p. 2517.
[31] T. Morse and C. Williamson, "Prediction of vortex-induced vibration response by employing controlled motion," *Journal of Fluid Mechanics*, vol. 634, p. 5, 2009.